scientific reports

Check for updates

OPEN

Folate receptor targeted nanoparticles containing niraparib and doxorubicin as a potential candidate for the treatment of high grade serous ovarian cancer

Lucy Wang, James C. Evans, Lubabah Ahmed & Christine Allen✉

Combination chemotherapy is an established approach used to manage toxicities while eliciting an enhanced therapeutic response. Delivery of drug combinations at specific molar ratios has been considered a means to achieve synergistic effects resulting in improvements in efficacy while minimizing dose related adverse drug reactions. The benefits of this approach have been realized with the FDA approval of Vyxeos®, the first liposome formulation to deliver a synergistic drug combination leading to improved overall survival against standard of care. In the current study, we demonstrate the synergistic potential of the PARP inhibitor niraparib and doxorubicin for the treatment of ovarian cancer. Through in vitro screening in a panel of ovarian cancer cell lines, we find that niraparib and doxorubicin demonstrate consistent synergy/additivity at the majority of evaluated molar ratio combinations. Further to these findings, we report formulation of a nanoparticle encapsulating our identified synergistic combination. We describe a rational design process to achieve highly stable liposomes that are targeted with folate to folate-receptor-alpha, which is known to be overexpressed on the surface of ovarian cancer cells. With this approach, we aim to achieve targeted delivery of niraparib and doxorubicin at a pre-determined synergistic molar ratio via increased receptor-mediated endocytosis.

Abbreviations

OC	Ovarian cancer
APH	Acid phosphatase
BSA	Bovine serum albumin
CI	Combination index
cryo-TEM	Cryogenic transmission electron microscopy
DL	Moles total drug:moles total lipid
DMSO	Dimethyl sulfoxide
DOX	Doxorubicin
dsDNA	Double stranded DNA
ELSD	Evaporative light scattering detector
EPR	Enhanced permeability and retention
folate-PEG_{5k}-DSPE	1,2-Distearoyl-sn-glycero-3-phosphoethanolamine-*N*-[folate(polyethylene glycol)-5000]
FRα	Folate receptor alpha
HBS	HEPES buffered saline
HGSOC	High grade serous ovarian cancer
HSPC	Hydrogenated soybean phosphatidylcholine
NIRB	Niraparib
NIRB-DOX	Untargeted niraparib and doxorubicin loaded liposomes
NIRB-DOX-CIT	Sodium citrate core liposomes loaded with niraparib and doxorubicin

Leslie Dan Faculty of Pharmacy, University of Toronto, 144 College Street, Toronto, ON M5S 3M2, Canada. ✉email: cj.allen@utoronto.ca

NIRB-DOX-FA	Folate targeted niraparib and doxorubicin loaded liposomes
OLP	Olaparib
PARPi	Parp inhibitor
PBS	Phosphate buffered saline
PEG_{2k}-DSPE	*N*-(Methylpolyoxyethylene oxycarbonyl)-1,2-distearoyl-sn-glycero-3-phosphoethanolamine with a 2000 molecular weight PEG chain
PEG_{5k}-DSPE	*N*-(Methylpolyoxyethylene oxycarbonyl)-1,2-distearoyl-sn-glycero-3-phosphoethanolamine with a 5000 molecular weight PEG chain
PLD	PEGylated liposomal doxorubicin
SEC	Size exclusion chromatography
TEA	Triethylamine
TEA_8SOS	Triethylammonium sucrose octasulfate

Ovarian cancer (OC) is the fifth leading cause of cancer related deaths among Canadian and American women, with the poorest five-year survival rates among all gynecological cancers[1,2]. Despite significant research in this area, patient survival outcomes have seen relatively small gains in survival rates with average age adjusted rates of death falling by merely 2.7% per year[3].

Nevertheless, within the past decade we have seen the first major innovation in OC treatment since the 1990s with the FDA approval of the first-in-class poly-ADP ribose polymerase (PARP) inhibitor (PARPi), olaparib (OLP). In 2014, OLP was approved as a monotherapy for patients with germline BRCA-mutated advanced stage OC who have undergone prior treatment with three or more chemotherapies (such as taxanes and platinum agents)[4]. OLP use has since been expanded to include maintenance therapy in recurrent OC patients who are either fully or partially responsive to platinum-based therapy[5].

PARPis are a family of molecular therapies that take advantage of the homologous recombination repair defects (i.e. the "BRCAness" phenotype) prevalent in the majority of high grade serous ovarian cancer (HGSOC) tumors to create a synthetic lethality effect[6,7]. There are currently three PARPis approved for the treatment of OC: OLP, rucaparib, and niraparib (NIRB), that differ with respect to their degree of PARP inhibition and PARP trapping[8,9].

To improve patient outcomes, there have been several studies aimed at determining the therapeutic potential of PARPis in combination with other chemotherapeutic and molecular therapy agents. Clinical trials that add PARPis to traditional first- or second-line OC chemotherapies have garnered mixed results with key limitations being dose limiting toxicities. These toxicities have been reported to be mainly hematological in nature and sometimes affect as many as two-thirds of the cohort at even low dosage levels[10–18]. Furthermore, recent work looking at combining PARPis with novel molecular therapies such as ATR and WEE1 inhibitors have found similar hematological toxicity drawbacks[19,20].

Although sequential combination therapy and the use of drug "holidays" have been proposed (and successfully applied) to overcome toxicity barriers, administration of concomitant drug combinations remains ideal for ease of clinical application and potential improvements in treatment efficacy. To address this clinical need, we propose to reduce PARPi related drug toxicities by pre-screening prospective PARPi-chemotherapy combinations in vitro for synergistic action. Identified candidate combinations would then be encapsulated together into a common nanoparticle for consideration for both passive and active delivery to cancer cells.

The benefits of nanoparticle mediated combination delivery combine the well documented reduced systemic toxicity effect of nanoparticle encapsulation with the ability to package and deliver optimized synergistic drug combinations at the relative ratio found to be most effective. This optimized "ratiometric" advantage to applying drug combinations is well documented in the literature[21–24]. Vyxeos is the first dual-encapsulated nanoparticle that uses this approach to treat acute myeloid leukemia. Delivering a synergistic 5:1 molar ratio of cytarabine and daunorubicin, Vyxeos is the only nanoparticle formulation to date that has demonstrated superior overall survival when compared to the standard of care (i.e., 7-day continuous infusion of cytarabine with 3-day infusion of daunorubicin)[25,26]. Furthermore, patients who received Vyxeos (as opposed to the standard of care) had significantly lower incidence of cardiac toxicity[27]. These outcomes provide the basis for our current approach to addressing the toxicity associated with PARPis when combined with traditional standard of care chemotherapy.

In the following we describe the in vitro screening of the PARPi NIRB in combination with the anthracycline doxorubicin (DOX) in a panel of OC cell lines. Using the Chou-Talalay method, we evaluated the synergistic potential between NIRB and DOX at various relative molar ratio combinations. In doing so, we found that NIRB and DOX exert consistent synergistic action at select molar ratios that is lost when homologous recombination (HR) repair is restored. Subsequently, we outline the rational design of an actively targeted, stable, dual-encapsulated NIRB and DOX liposome for the treatment of HGSOC. Graphically summarized in Fig. 1, this is (to our knowledge) the first reported dual loaded liposome that entraps a PARPi and a chemotherapeutic agent. The reported discovery is an important first step towards our ability to safely use PARPi combinations concurrently in the clinic and fulfil a current unmet need.

Results

NIRB and DOX drug combination screening. To elucidate the synergistic potential of our test compounds, NIRB and DOX were combined at varying relative molar ratios and screened for cytotoxicity in a panel of representative HGSOC cell lines. The combination index (CI) values were determined using the synergy determination software, CompuSyn. Thresholds for synergism, additivity, and antagonism were set at ≤ 0.9, between 0.9 and 1.1, and ≥ 1.1, respectively.

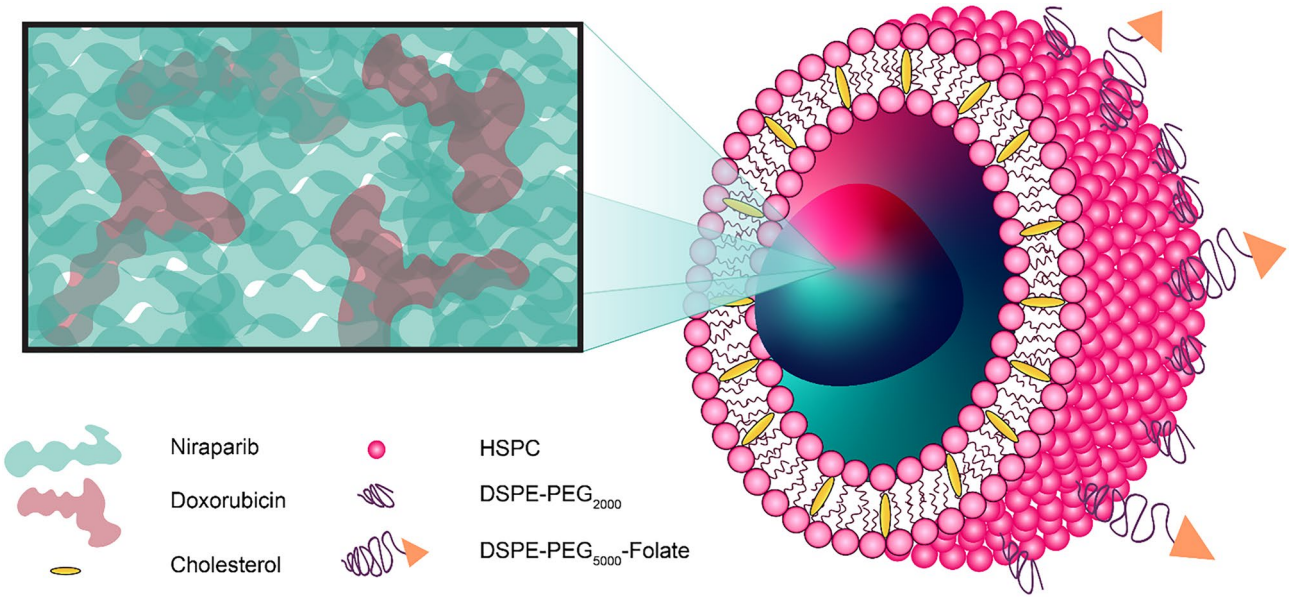

Figure 1. Graphical schematic of the presented synergistic, actively targeted, dual encapsulated NIRB and DOX liposome. The formulated nanoparticle is designed and optimized to deliver a pre-screened, synergistic combination of NIRB and DOX to HGSOC cancer cells. This is, to our knowledge, the first reported dual loaded PARPi and DOX liposome of its kind.

NIRB:DOX Fa=0.5

	20:1	10:1	5:1	2:1	1:1	1:2	1:5	1:10	1:20
OVCAR8	0.95	0.79	1.08	0.99	0.89	0.89	1.06	1.04	0.94
HEYA8	0.92	0.75	0.85	0.96	0.82	0.95	1.09	1.05	0.88
PEO1	1.01	0.82	0.96	0.96	0.93	1.03	0.79	0.87	0.81
PEO4	1.21	0.85	1.00	0.90	0.97	1.16	1.09	1.18	1.04

NIRB:DOX Fa=0.75

	20:1	10:1	5:1	2:1	1:1	1:2	1:5	1:10	1:20
OVCAR8	0.97	0.90	1.01	1.09	0.91	0.99	0.99	0.97	0.96
HEYA8	0.87	0.89	0.92	0.99	0.89	1.07	1.03	1.00	0.93
PEO1	0.89	0.93	0.94	0.93	0.96	1.01	0.92	0.96	0.89
PEO4	1.27	1.08	1.08	1.06	1.13	1.18	1.15	1.14	0.99

Table 1. Heat map showing mean CI values at (A) Fa = 0.5 and (B) Fa = 0.75 for treatments of NIRB:DOX at varying relative molar ratios in a panel of four HGSOC cell lines. CI values ≤ 0.9 indicates synergistic effects (green), 0.9 > CI < 1.1 indicates additive effects (yellow), and CI ≥ 1.1 indicates antagonistic effects (red). The 10:1 molar ratio is shown to have consistent mean synergistic/additive effects in all cell lines at both Fa = 0.5 and Fa = 0.75. CI values were calculated using CompuSyn software.

As shown in Table 1, CI values obtained for ratiometrically combined NIRB and DOX combinations applied to cell monolayers showed a general trend of mean additivity for all applied molar ratios at both fractions affected (Fa) 0.5 and 0.75 (i.e., 50% and 75% cell death, respectively). Interestingly, pockets of mean antagonism were exclusively observed in the PEO4 cell line, a platinum resistant sister pair to the PEO1 cell line.

As such, the 10:1 NIRB:DOX ratio was the only test mixture that showed consistent mean synergy across all tested cell lines at Fa = 0.5 with only a slight increase in CI value towards mean additivity at Fa = 0.75.

Expressed as a scatter plot, Fig. 2 shows that the standard deviations for biological replicates of the 10:1 ratio consistently remain in the synergistic and additive range for all cell lines except PEO4. PEO4 was also found to be the only cell line where variability for all tested ratiometric mixes deviated into the antagonistic region, a detail that is not conveyed when solely looking at mean values.

Cell surface expression of folate receptor alpha (FRα) and cellular uptake of folate conjugated liposomes. Given that 70% of primary and 80% of recurrent HGSOC tumors overexpress FRα, the folic acid

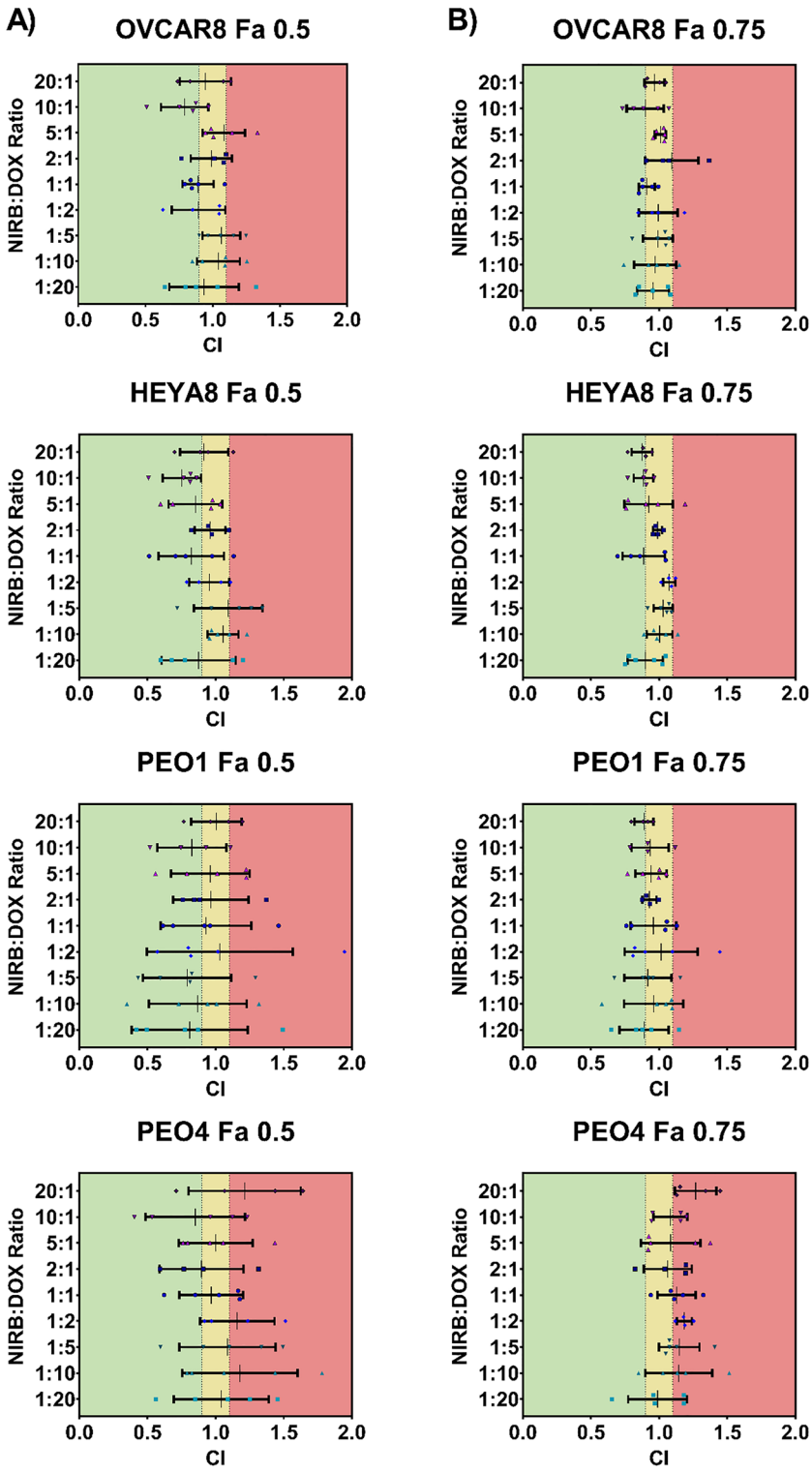

Figure 2. Scatter plot showing mean ± SD CI values at (**A**) Fa = 0.5 and (**B**) Fa = 0.75 for treatments of NIRB:DOX at varying relative molar ratios on a panel of four HGSOC cell lines. CI values ≤ 0.9 indicate synergistic effects (green), 0.9 > CI < 1.1 indicate additive effects (yellow), and CI ≥ 1.1 indicate antagonistic effects (red). The 10:1 molar ratio is shown to have consistent synergistic/additive effects in all cell lines at both Fa = 0.5 and Fa = 0.75 except for PEO4, wherein the combination of NIRB and DOX seems to exhibit a wide range of values including those indicative of antagonism across the various molar drug ratios. CI values were calculated using CompuSyn software.

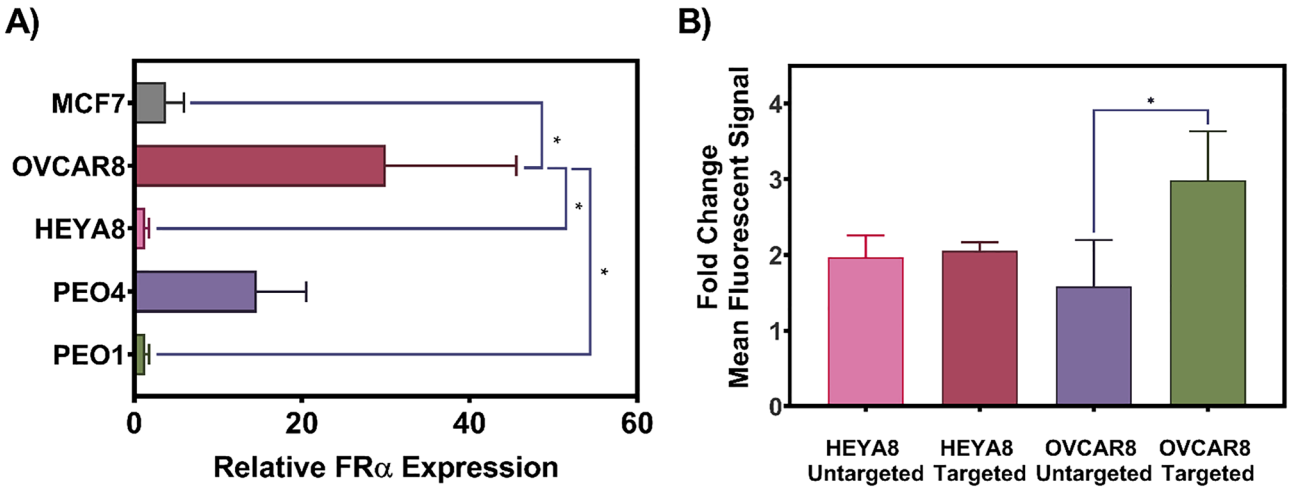

Figure 3. (**A**) Relative FRα expression in the selected panel of OC cell lines with MCF7 (breast cancer cell line) as a negative control and (**B**) Cellular uptake of folate conjugated versus unconjugated fluorescent calcein loaded liposomes. Flow cytometry was used to confirm the relative expression of FRα in the panel of OC cell lines. Data is presented as mean FITC for treated cells divided by the mean FITC for untreated cells, *$p < 0.05$ ($n = 3$). Flow cytometry was used to determine the uptake of folate conjugated and folate unconjugated calcein-loaded liposomes in FRα high (OVCAR8) and low (HEYA8) expressing cells, presented as mean FITC values. Data is presented as mean FITC for treated divided by the mean FITC for untreated cells, *$p < 0.05$ ($n = 3$).

small molecule was identified as a potential active targeting ligand[28]. Per Fig. 3A, surface expression of FRα on the selected panel of OC cell lines was measured by flow cytometry with the breast cancer cell line MCF7 used as a negative control. The OVCAR8 cell line was found to have significantly higher FRα expression compared to both the negative control, HEYA8, and the PEO1 cell line. OVCAR8 was thus selected to evaluate the suitability of our carrier for in vitro cellular uptake.

As shown in Fig. 3B, cellular uptake of folate conjugated, fluorescent probe encapsulating liposomes into OVCAR8 cells was significantly greater than unconjugated control liposomes. This effect was not observed in the HEYA8 cell line which does not overexpress surface FRα.

NIRB and DOX dual loading optimization. Dual loading of NIRB and DOX into a common liposome was pursued to deliver a controlled, synergistic ratio of both drugs to cancer cells. Remote drug loading using a pH gradient and triethylammonium sucrose octasulfate (TEA_8SOS) as an internal entrapment agent was selected as the method of choice. NIRB and DOX were added to blank liposomes at varying relative molar ratios to study the dual loading pattern and to determine if one drug loads preferentially into liposomes in comparison to the other. Successfully entrapped NIRB:DOX molar ratios were plotted as a function of added NIRB:DOX molar ratios to elucidate a potential relationship (Fig. 4).

Dual, active loading of NIRB relative to DOX into the TEA_8SOS enriched core of blank liposomes was found to be reproducible. This relationship can be described linearly wherein increasing the added proportion of NIRB relative to DOX at the active loading step incrementally increased the encapsulated amount of NIRB relative to DOX in a predictable manner. This linear relationship can be expressed as $y = 1.10x - 0.178$ between the tested limits.

According to the relationship determined by the plot, substituting $y = 10$ (i.e., desired encapsulated NIRB:DOX ratio), the required ratio of added NIRB:DOX was determined to be 9.25:1. Applying this experimentally, the resultant folate conjugated liposomes (NIRB-DOX-FA) reproducibly encapsulated 9.4 ± 0.6:1 molecules of NIRB relative to DOX. Table 2 shows a summary of the characteristics of these folate conjugated and drug loaded liposomes.

NIRB-DOX-FA liposome in vitro characterization. The in vitro release of drug from the NIRB-DOX-FA liposomes was evaluated under sink conditions that mimic blood serum (Fig. 5A). Timepoints collected were 0-h (i.e., sample run down the size exclusion column immediately after addition of release media to purified liposomes), 1-h, 2-h, 4-h, 6-h, 10-h, 24-h, 48-h, 72-h, 96-h, and 120-h.

As shown in Fig. 5B, the NIRB:DOX molar ratio was maintained within 7.3 ± 1.1 throughout the entire 5-day study period. This observed NIRB:DOX ratio deviates from the target 10:1 synergistic ratio but remains within the synergistic/additive range for all cell lines. This discrepancy is a result of variable relative drug recovery during the extraction process wherein DOX was more efficiently recovered from the in vitro release media components than NIRB—hence necessitating a time 0-h control group.

When all timepoints are compared to 0-h (NIRB:DOX ratio 7.1 ± 0.3), there were no statistically significant changes in encapsulated ratio. As such, relative to timepoint 0-h, it is concluded that there was no measurable release of drug payload over a 5-day incubation period.

Cryo-transmission electron microscopy (cryo-TEM) of unloaded vs loaded liposomes were conducted to elucidate the particle morphology of the dual drug loaded liposomes. Representative images of the drug

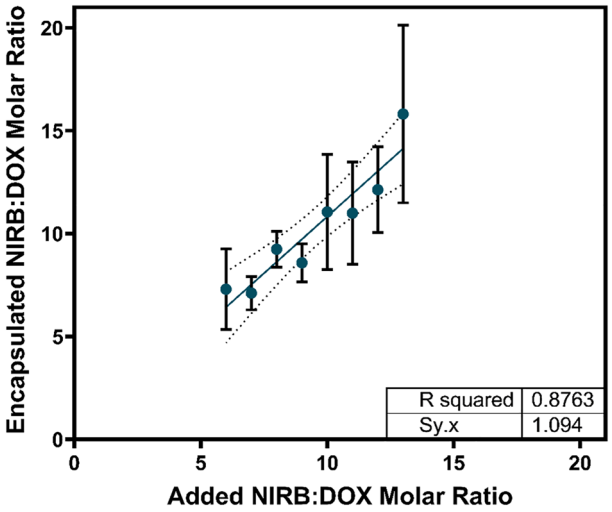

Figure 4. Relationship between the added molar ratio of NIRB:DOX and the corresponding resulting "encapsulated molar ratio" following active loading with TEA_8SOS as a trapping agent. DOX and NIRB concentrations in the resultant liposomes were quantified by mass spectrometry. Increases in relative molar ratios of encapsulated NIRB:DOX can be linearly related to increases in relative molar ratios of added NIRB:DOX. The determination of this relationship allowed for the formulation of a synergistic NIRB:DOX liposome in a predictable and reproducible fashion. Data is presented as mean ± SD with the dotted lines denoting the 95% confidence interval (n = 3).

Size (nm)	Encapsulation efficiency (%)		Drug:lipid molar ratio	Resultant NIRB:DOX molar ratio
	NIRB	DOX		
124.6 ± 53.9	87.6 ± 19.9	71.5 ± 17.3	0.4 ± 0.1	9.4 ± 0.6:1

Table 2. Size, encapsulation efficiency, and drug to lipid ratio of the optimized, folate conjugated, lead liposome candidate, NIRB-DOX-FA. Nanoparticle size was determined by DLS. NIRB and DOX concentrations were determined by HPLC–UV analysis and lipid quantification was performed by HPLC-ELSD.

loaded liposomes reveal dark areas of high electron density that are not present in unloaded liposomes (Fig. 6). Using ImageJ software to analyze the mean gray area difference across the phospholipid membrane of loaded vs unloaded liposomes reveals that drug loading results in a significant increase in mean gray area difference across the liposomal membrane (Fig. 7)[29]. In addition, drug loading and entrapment using the TEA_8SOS agent is shown to change the liposomal morphology from a circular to an oblong shape.

Discussion

Synergy in the NIRB and DOX combination is both ratiometrically and homologous recombination repair proficiency dependant. The NIRB:DOX combination demonstrated consistent mean additivity with regions of synergy for most molar ratios tested across all cell lines with the exception of the PEO4 cell line (Table 1). Among the screened molar drug ratios, the 10:1 molar ratio of NIRB:DOX demonstrated the most consistent synergistic effect across most cell lines, highlighting 10:1 as a combination candidate for nanoparticle delivery. Synergy of the 10:1 ratio remains true when looking at CI values in terms of mean ± SD (Fig. 2). While the variability of CI values for most applied NIRB:DOX molar ratios include antagonism, the CI standard deviation of the 10:1 ratio consistently falls within the synergistic/additive range for all cell lines except for PEO4.

Though the mechanism by which the NIRB and DOX combination results in either synergy or antagonism is not fully understood, it is hypothesized that the combination of DOX and NIRB could exhibit synergy via the creation of double stranded DNA (dsDNA) breaks. Previous work exploring the synergistic mechanisms of DOX when combined with another PARPi, OLP, revealed that the PARPi-anthracycline combination results in its synergistic cytotoxicity by creating more dsDNA breaks than either drug applied as a monotherapy[30]. Though comparative mechanistic studies have not been conducted with NIRB and DOX, given the PARP trapping and inhibition similarities between OLP and NIRB, it is possible that the NIRB and DOX combination exhibits synergy via similar mechanisms[31].

Furthermore, closer examination of the synergistic potential of the NIRB:DOX combination when applied to PEO4 reveals a general trend towards antagonism at all tested molar ratios. These results were consistent with

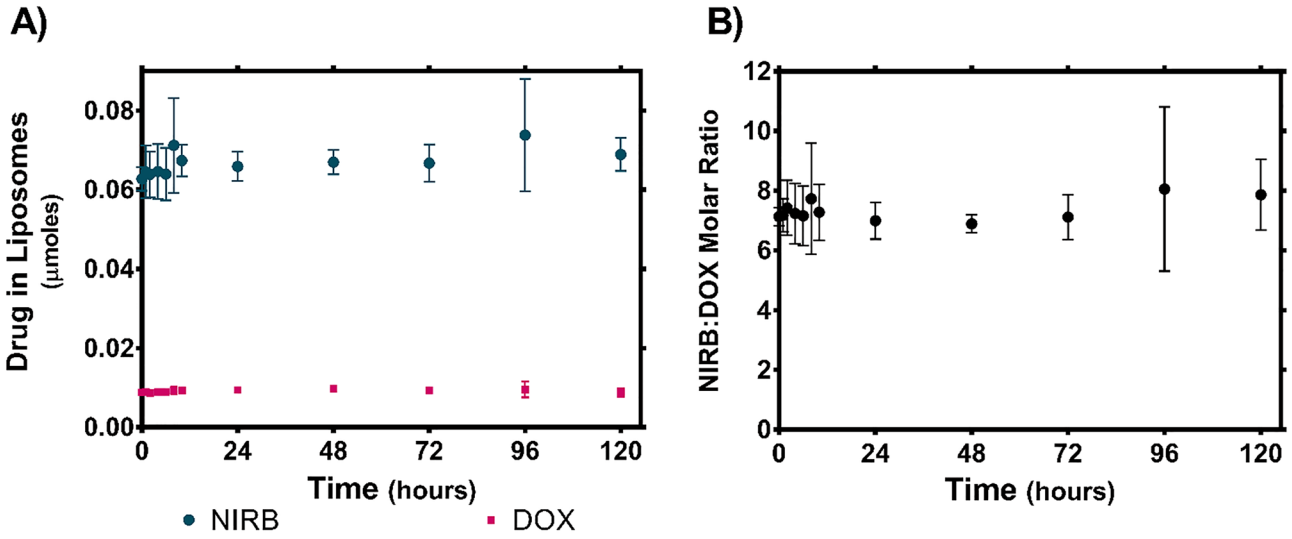

Figure 5. (**A**) In vitro release of NIRB and DOX from NIRB-DOX-FA in bovine serum albumin (BSA) enriched buffer and the (**B**) corresponding encapsulated NIRB:DOX molar ratio. The y-axis shows the mean absolute value (μmoles) of NIRB and DOX remaining in the liposomes (± SD) within collected 100μL fractions when NIRB-DOX-FA liposomes are subjected to biologically relevant (i.e., 50 mg/mL BSA, pH 7.4, 37 °C) sink conditions over five days. Virtually no drug was released between time 0-h and 120-h, resulting in the maintenance of initial versus final NIRB:DOX molar ratios (7.13 ± 0.30:1 at time 0-h and 7.86 ± 1.19:1 at time 120-h). Data is presented as mean ± SD (n = 3).

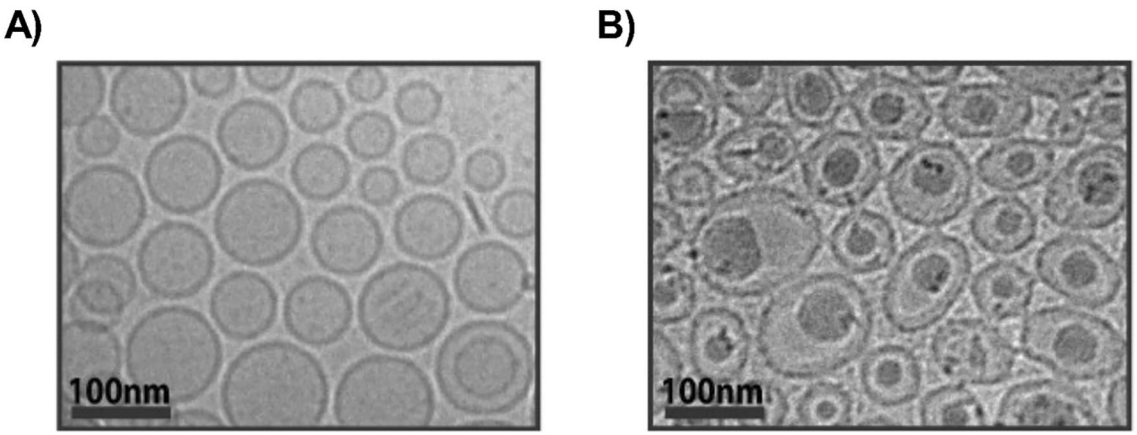

Figure 6. Cryo-TEM images of (**A**) unloaded TEA_8SOS liposomes and (**B**) NIRB and DOX loaded TEA_8SOS liposomes. Darker versus lighter areas demonstrate the presence of a greater versus lower electron density, respectively. Comparing images of loaded versus unloaded liposomes, drug loaded liposomes exhibit dark, electron dense deposits at the core. These deposits may be due to precipitated drug in the liposomal core.

previous work done in our group which showed a similar antagonistic pattern with the OLP and DOX combination across all tested molar ratios[30]. These findings are in stark contrast to the synergistic/additive profile of the NIRB and DOX combination shown in the PEO1 cell line.

This comparison is critical to our understanding of PARPi and DOX combinations as PEO1 and PEO4 are sister cell lines that were derived from the same patient at different points of disease progression. The PEO1 cell line was obtained from the patient at the stage of primary tumor debulking following one round of neoadjuvant chemotherapy (cisplatin, 5-FU, and chlorambucil) while the PEO4 cell line was derived from bulk tumor removed during the secondary tumor debulking after the development of clinical resistance to the aforementioned chemotherapy[32]. Inspection of the PEO1 and PEO4 sister pair reveals a BRCA2 mutation reversion to wild-type that is present in the PEO4 cell line[33]. Given that BRCA2 works exclusively on the HR repair pathway, we hypothesize that the observed synergy for the NIRB and DOX combination is highly dependent on HR repair deficiency[34]. However, additional studies are needed to support this hypothesis.

These results suggest that a synergistic effect for the combination of NIRB and DOX is both cell line and molar ratio dependent. Translation of this combination to the clinic would thus likely need to be in conjunction with criteria for identifying patients likely to respond to this therapy. In the case of OLP, during AstraZeneca's 2014 Phase I trial, the oral PARPi OLP and intravenous (IV) pegylated liposomal doxorubicin (PLD) combination

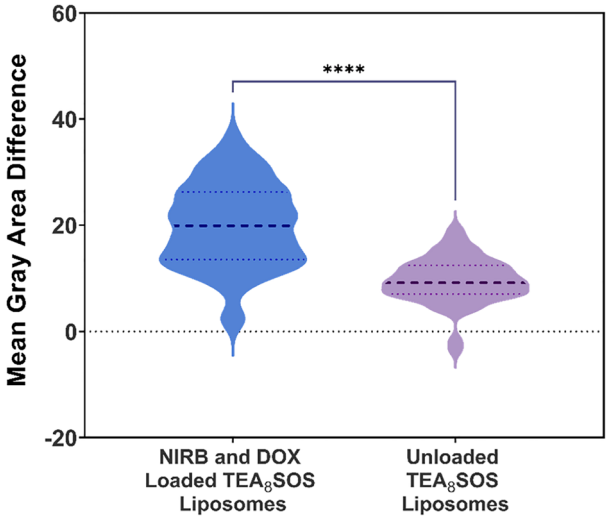

Figure 7. Differences in mean gray area of the exterior versus interior of drug loaded (NIRB-DOX-FA) and unloaded TEA_8SOS liposomes. Mean gray area is defined as the average photo intensity divided by the number of pixels in a selected image area. Mean gray area was determined to quantify the darkened electron dense areas at the core of NIRB-DOX-FA liposomes versus unloaded liposomes. As such, statistically significant differences in mean gray area across the bilayer of NIRB-DOX-FA liposomes, relative to unloaded liposomes, highlights the presence of electron dense drug deposits after active drug loading. Mean gray area of the liposomes was determined by ImageJ software for the cryo-TEM images. Data is presented as differences in mean gray area ($n = 56$ liposomes, $^{****}p < 0.0001$).

elicited either a complete or partial response in only 25% of platinum resistant patients as opposed to the observed 71% for platinum sensitive patients[35]. The present study aimed to investigate whether a ratiometric approach to PARPi and DOX combinations would yield drug synergy, potentially bridging the difference in observed response rate between platinum sensitive and resistant disease. Based on the limited number of cell lines evaluated, HR repair proficient tumors may be an exclusion criterion for this treatment strategy where BRCA status may be used to identify good vs bad responders. However, this warrants further investigation.

Clinical trials conducted on oral NIRB (Zejula®) and IV PLD in patients with platinum resistant/refractory HGSOC have been attempted. It was hypothesized that the combination of Zejula and PLD would result in either a "tumor response rate equal or superior to that of historical data for [PLD] alone" or a reduction in "number of participants with dose-limiting toxicities" (NCT01227941). This study has since been terminated with no publication on the findings from the trial.

Though it is not known why this specific trial was terminated, given that BRCA reversion is a known mechanism of treatment resistance (particularly after routine PARPi therapy), it is possible that random recruitment of refractory HGSOC cohorts results in inclusion of patients with HR proficient tumors[36]. Since our findings suggest that HR deficiency is a preliminary requirement for the synergistic action of PARPi and DOX, heterogenous inclusion of all platinum resistant patients could result in non-significant changes in primary outcome measures.

This points to the need to better understand how next generation molecular therapies affect cancer cell biology, particularly in the pathological reality of intervention induced genomic instability. The HR repair pathway and its relation to the larger, overall DNA damage response (DDR) network is vastly complex. As such, our work to capitalize on the innate repair deficiencies that are present in cancer cells with not one, but a cocktail of modern-day therapeutics must be further mechanistically studied to better inform clinical decisions.

Active targeting ensures cellular uptake of synergistic payload. One of the marked issues with applying combination drug therapies at specific optimized ratios is delivery. While physiological challenges consist of differing pharmacokinetic and biodistribution (PKBD) properties of each individual compound (both separately and when administered together), the cellular challenge consists of controlling for and ensuring cellular uptake at the suggested ratio. For both barriers to implementation, targeted delivery of a dual loaded nanoparticle provides a feasible solution. While encapsulation of optimized drug combinations regulates the PKBD characteristics of the drug cocktail to a singular profile, active targeting for cellular uptake ensures controlled cell uptake of the optimized ratio.

As such, active targeting using the folic acid small molecule was pursued. As mentioned previously, the cell surface FRα receptor is overexpressed in the majority of both primary and recurrent HGSOC tumors. The selection of FRα as the target of choice was informed by literature demonstrating enhanced efficacy of folate receptor targeted formulations in preclinical animal models relative to their untargeted controls[37–39]. In the clinical setting, novel therapeutics targeting FRα have seen success. A notable example in this category includes mirvetuximab/IMGN853, an antibody drug conjugate that led to significant improvements in secondary outcomes in phase III clinical trials[40].

To assess whether folate targeting can facilitate improved cellular uptake of dual-loaded liposomes into FRα overexpressing cells, the expression status of FRα in the OC cell panel was determined in order to identify an appropriate FRα overexpressing model. As shown in Fig. 3A, the OVCAR8 cell line exhibited significantly higher levels of FRα expression relative to the MCF7 negative control ($p < 0.01$). In contrast, none of the other cell lines evaluated (i.e., HEYA8, PEO1/4) demonstrated enhanced expression of FRα relative to MCF7.

Given the FRα expression profiles, cellular uptake of folate conjugated versus unconjugated liposomes was then evaluated in the FRα overexpressing OVCAR8 cells versus the FRα non-overexpressing HEYA8 cells. Statistically significant increases in cellular uptake of folate conjugated versus unconjugated liposomes in the OVCAR8 cell line compared to the HEYA8 cell line confirmed that our carrier lipid composition and active folate targeting strategy are effective at improving liposomal payload uptake into FRα overexpressing cells.

Optimized liposomal dual encapsulation of NIRB:DOX capitalizes on observed synergy. Given that the observed in vitro combination results only demonstrated consistent pronounced synergy at a 10:1 molar ratio (NIRB:DOX), it was imperative that this molar ratio be delivered to cancer cells with little deviation. To achieve this, liposomal core composition was optimized to deliver a controlled amount of each drug into OC cells.

As described in a review on nanocrystallization by the Boyd group, the physical state of drug at the nanoparticle core can significantly influence its release kinetics. A solid core morphology has been shown to slow the rate of drug release[41]. This phenomenon has been extensively studied for DOX loaded liposomes and the crystal structure of the resulting drug precipitates[42]. It was hence hypothesized that, to achieve minimal systemic drug release, the proposed NIRB-DOX co-encapsulated formulation would benefit from a more solid core morphology.

With regards to ionizable drugs such as NIRB and DOX, it was prudent to explore gradient mediated active loading using entrapment salts such as TEA_8SOS. Developed by Drummond and colleagues, the TEA_8SOS entrapment agent has been shown to form stable complexes with irinotecan cations[43]. Other groups studying salt variations in irinotecan gradient loading have also found that the use of TEA_8SOS creates liposomes of superior stability when challenged in vitro, possibly due to sucrose octasulfate's ability to promote "inter-fiber crosslinking" by interacting with multiple drug cations simultaneously[44]. These positive findings in the literature thus encouraged the pursuit of similar results for other drug cations such as NIRB and DOX.

To explore the potential utility of TEA_8SOS as an effective trapping agent, it was important to determine whether NIRB and DOX could be co-loaded into TEA_8SOS enriched core liposomes at the 10:1 molar ratio in a reproducible fashion. As shown in Fig. 4, incremental increases in added NIRB relative to DOX resulted in incremental increases in encapsulated levels of NIRB and DOX that can be described using a linear regression.

Alternative, non-linear models were explored with the aim of better understanding the loading characteristics of NIRB relative to DOX using TEA_8SOS as an entrapment agent (Supplementary Fig. S1). As a result, a third-order polynomial regression was found to better model the dual loading characteristics of NIRB and DOX under the TEA_8SOS gradient conditions between the tested molar ratios. However, for each of the regression models investigated to achieve an encapsulated molar ratio of 10, the values for added molar ratio obtained were similar to each other and to those afforded by the linear regression model. For instance, the exponential equation predicted 9.56, the second-order polynomial predicted 9.32, and the third-order polynomial equation predicted 9.95. In addition, the 95% confidence windows of the prediction are shown to increase for all regression models as we attempt to achieve incrementally higher encapsulated NIRB:DOX molar ratios, suggesting potentially poorer reproducibility when formulating liposomes with higher NIRB content relative to DOX.

Nevertheless, given that areas of narrower 95% confidence intervals encompass the desired 10:1 NIRB:DOX molar ratio, the initial, simple linear regression model of the relative NIRB:DOX drug loading relationship was selected for simplicity of use and robustness of transferability. This prediction was experimentally validated and led to the resulting NIRB-DOX-FA liposomes encapsulating 9.4 ± 0.6:1 of NIRB:DOX, confirming TEA_8SOS's reproducible ability to co-entrap both drugs at adequate efficiencies.

It should be noted that pH gradient mediated active loading using sodium citrate (NIRB-DOX-CIT) as an intraliposomal entrapment agent was also attempted given its frequent use in the preparation of DOX containing liposomes[45]. Entrapment using sodium citrate, however, yielded NIRB and DOX liposomes with in vitro release characteristics that were less favorable than that of the current candidate, as shown in Supplementary Fig. S2. Specifically, co-encapsulation of NIRB and DOX into the core of sodium citrate liposomes resulted in rapid in vitro release. While NIRB-citrate liposomes maintained approximately 50% of their drug cargo after 120 h of incubation (Supplementary Fig. S3), NIRB-DOX-CIT liposomes exhibited rapid release (~62% DOX and ~85% NIRB) at the 24-h timepoint (Supplementary Fig. S2). We thus concluded that sodium citrate was an unsuitable entrapment agent for the co-loading of NIRB and DOX into liposomes.

Cryogenic electron microscopy of NIRB-DOX liposomes reveal presence of an electron-dense drug core. Cryo-TEM images of NIRB-DOX-FA liposomes were taken to determine the morphology of both drugs in the liposomal core. As previously noted, a solid core is desirable to minimize drug release from FRα targeted liposomes while in systemic circulation. Cryo-TEM images of unloaded and dual loaded TEA_8SOS liposomes presented in Fig. 6B show that drug loading results in the formation of dark, electron-dense deposits in the liposomal core.

As shown in Fig. 7, calculated mean gray value differences on the inside versus outside of NIRB-DOX-FA liposomes were found to be significantly larger than that of unloaded TEA_8SOS core liposomes ($p < 0.0001$), suggesting the presence of large, concentrated amounts of co-encapsulated drug within the internal volume of the liposomes. Since cryo-TEM imaging measures electron density, darker visible regions in the images represent areas of high concentrations of encapsulated drug. According to the work performed by others on DOX loaded

liposomes, this suggests the presence of drug precipitate which likely gives rise to the observed stability of the drug loaded liposomes[42].

Interestingly, per Supplementary Fig. S5, NIRB-DOX-FA exhibited a statistically significant increase in mean gray difference when compared to NIRB-DOX-CIT, suggesting a difference in sodium citrate's ability to enable drug precipitation when compared to TEA_8SOS. It should also be noted that internal media concentrations of anions for NIRB-DOX-CIT and NIRB-DOX-FA liposomes are 900 mEq and 650 mEq, respectively. As such, despite providing more available anions for electrostatic interactions with drug cations, sodium citrate was unable to facilitate drug precipitation relative to TEA_8SOS, pointing towards sucrose octasulfate's structural ability to induce drug precipitation which reduced the rate of drug release.

NIRB-DOX-FA liposomes exhibit sustained in vitro release profiles. In vitro release studies (Fig. 5) in the presence of BSA (50 mg/mL in pH 7.4 HEPES buffered saline at 37 °C) revealed that NIRB-DOX-FA liposomes exhibited no statistically significant amount of drug release over the duration of the study (comparing encapsulated drug levels at $t = 0$ h vs $t = 120$ h, $p = 0.9$ and $p = 1.0$ for NIRB and DOX, respectively). At the 120-h timepoint, the encapsulated NIRB:DOX molar ratio remained close to the synergistic target.

As highlighted above, it is hypothesized that the observed high level of payload stability is due to the co-precipitation of both NIRB and DOX within the liposomal core. Precipitation has been shown to slow the release kinetics of drugs[41,44]. Had NIRB and DOX not formed intraliposomal drug precipitates, in vitro drug release would have likely followed a more rapid Fickian profile (i.e., due to drug release being governed by the concentration gradient across the liposome membrane)[46]. Thus, the hypothesis that NIRB-DOX-FA liposomes exhibit a solid core offers a more plausible explanation for their slow-release profile since drug release would additionally be governed by solid drug dissolution. Further characterization studies using techniques such as x-ray diffraction would be required to objectively confirm the state of the intraliposomal drug molecules.

Inherent stability of the dual-loaded formulation is ideal for active targeting to the characteristically over-expressed FRα to ensure controlled delivery of the identified synergistic ratio. Successful application of the active targeting strategy was similarly employed by Merrimack Pharmaceuticals Inc. for MM-302, a liposomal formulation of DOX actively targeted to the HER-2 receptor. As shown in the case of MM-302, active targeting leads to increased tumor cell uptake of the liposomes via receptor mediated endocytosis and improvement in the overall therapeutic effect[47,48].

Conclusion

At present, the above findings are the first (to our knowledge) to show synergistic effects for the combination of NIRB and DOX. Through our screening, we have found that the synergistic action of NIRB and DOX is both molar ratio and cell line dependent. NIRB and DOX, applied at a 10:1 relative molar ratio, exhibit consistent synergistic or additive effects for all tested HR deficient cell lines.

Perhaps the most important finding of this study was that the DOX and PARPi combination can lead to antagonism in cell lines with HR proficiency (i.e., intact BRCA2 function). In PEO4, the NIRB and DOX combination showed antagonistic effects across all applied molar drug ratios. These findings are in agreement with that of previous work done on the OLP and DOX combination by our group wherein mean CI values were found to be consistently higher in PEO4 versus PEO1[30]. Our screening therefore suggests that combinations of DOX and PARPis in general may be inappropriate for patients with HR proficient tumors—highlighting the need to better understand the action of not just monotherapies but drug combinations on cancer cell biology.

Combined delivery of drugs using nanoparticles is one of the only ways to achieve ratiometric combinations at diseased sites in vivo. Formulation of an optimal dual encapsulated nanoparticle brings to the forefront an additional set of considerations. Details such as dual drug retention and release require meticulous optimization to obtain the ideal candidate formulation.

In this study, we demonstrate the feasibility of developing a highly stable nanoparticle containing a synergistic, 10:1 molar ratio of NIRB:DOX actively targeted with folate to promote receptor mediated endocytosis and thus precision delivery of the molar drug ratio of interest. The formulation was designed through considering distinct drug entrapment techniques rather than optimization of the lipid composition. To our knowledge, this is the first time NIRB and DOX have been successfully co-encapsulated into a single nanoparticle.

Caveats to this study include the small number of OC cell lines screened. Screening the NIRB and DOX combination in a larger panel of OC cell lines (including additional platinum resistant cell lines) could identify the combination's performance in a broader range of settings that better model disease heterogeneity. As shown in our results with PEO1 versus PEO4, drug combination performance can be altered noticeably with either the functional loss or gain of one single gene. Evaluation of drug combinations in diverse cell lines with key mutations is thus crucial to elucidate the clinical characteristics of potential good versus bad responders.

Materials and methods

Materials. Hydrogenated soybean phosphatidylcholine (HSPC), *N*-(Methylpolyoxyethylene oxycarbonyl)-1,2-distearoyl-sn-glycero-3-phosphoethanolamine with a 2000 molecular weight PEG chain (PEG_{2k}-DSPE) and a 5000 molecular weight PEG chain (PEG_{5k}-DSPE) were purchased from NOF America Corporation (Kanagawa, Japan). Cholesterol was sourced from Corden Lipids (Plankstadt, Germany). 1,2-distearoyl-sn-glycero-3-phosphoethanolamine-*N*-[folate(polyethylene glycol)-5000] folate-PEG_{5k}-DSPE) was purchased from Nanocs (New York, USA). DOX HCl and NIRB free base were purchased from Tongchuan Pharma (Wujiang City, Jiansu, China). Sodium sucrose octasulfate was purchased from Toronto Research Chemicals (North York, Canada). Human OC cell lines were obtained as follows: PEO1 and PEO4 (ECACC, Public Health England, Salisbury, UK) were purchased from Sigma-Aldrich; HEYA8 was obtained from M.D. Anderson Cancer Center (Houston,

USA); OVCAR8 was obtained from the National Cancer Institute (Biological Testing Branch, NCI, MD, USA). All cell lines were authenticated using STR profiling by the Centre for Applied Genomics Genetic Analysis Facility (TCAG, Toronto).

In vitro combination cytotoxicity studies. A panel of four OC cell lines were selected for drug combination screening. Cells were seeded onto 96-well plates at the seeding densities listed in Table 3. Cells were left to adhere for 24 hours before undergoing a 72-h treatment with NIRB and DOX both as monotherapies and in combination at varying molar ratios of NIRB relative to DOX. Cellular viability was then measured using the acid phosphatase (APH) assay as described previously[30]. Briefly, 2 mg/mL of phosphatase substrate (Sigma Aldrich, Oakville, ON, Canada) was added to 0.1 M sodium acetate buffer, pH 5.5 with 0.1% Triton-X-100 and heated to 37 °C. Drug containing media was removed followed by a wash with warm phosphate buffered saline pH 7.4 (PBS) prior to the addition of 100µL of warm phosphatase supplemented buffer. The plates were then incubated at 37 °C for 2 hours followed by the addition of 10µL of 1 M sodium hydroxide to stop the reaction. The UV absorbance was then read on a Cytation-5 plate reader at 405 nm (BioTek, Winooski, VT, USA). Fraction affected was calculated as follows:

$$Fraction\ Affected = 1 - \frac{Absorbance_{Treatment} - Absorbance_{Media}}{Absorbance_{Control} - Absorbance_{Media}} \tag{1}$$

Total treatment concentration and the corresponding effects of NIRB and DOX both as monotherapies and varying relative molar ratios were inputted into CompuSyn software to obtain the CI values of the treatments for fractions affected 0.5 and 0.75 ($f_a = 0.5$ and $f_a = 0.75$, respectively).

Developed by the Chou group, CompuSyn utilizes the median-effect equation to determine the Hill-type coefficient (m) and the dose required to induce a median cytotoxicity effect (D_m) for both drugs singularly and in combination:

$$\frac{f_a}{f_u} = \left(\frac{D}{D_m}\right)^m \tag{2}$$

The median effect equation can be further manipulated to provide the basis of the median-effect plot:

$$\log\left(\frac{f_a}{f_u}\right) = m log\left(\frac{D}{D_m}\right) \tag{3}$$

From the median effect plot, CompuSyn then calculates the doses of drug 1, drug 2, and the drugs in combination (i.e., $(D_x)_1$, $(D_x)_2$, and $(D_x)_{1,2}$, respectively) that elicit x fraction affected. These values are then inputted into the following equation to calculate the CI value at varying fractions affected[49]:

$$CI = \frac{(D)_1}{(D_x)_1} + \frac{(D)_2}{(D_x)_2} \tag{4}$$

where $(D)_1$ and $(D)_2$ are the doses of drugs 1 and 2 required to elicit fraction affected x when applied in combination. The resulting CI value quantitatively defines the combined dose molar ratio wherein CI values < 1 are considered synergistic, equal to 1 additive, and > 1 antagonistic. In practice, CI values representing synergy, additivity, and antagonism are herein conservatively defined as ≤ 0.9, between 0.9 and 1.1, and ≥ 1.1 respectively[30].

Evaluating FRα expression in panel of cell lines. FRα expression in the panel of OC cell lines was determined using flow cytometry. Briefly, the chosen panel of OC cell lines as well as the breast cancer cell line, MCF7 (used as a negative control) were plated onto 24-well plates overnight at a seeding density of 1.24×10^5 cells per well[53]. Cells were left to adhere for 24 hours before being scraped and collected. Treatment groups were incubated with an anti-FRα primary antibody (1:100, ab3361, Abcam, Toronto, ON, Canada) while control group cells were incubated with PBS at 4 °C for 30 min. Cells were then pelleted via centrifugation, washed twice with ice cold PBS before incubation with the Alexa Fluor® 488-labelled secondary antibody (1:2000, ab150113, Abcam, Toronto, ON, Canada) for another 30 min. After treatment with the secondary antibody, cells were pelleted and washed twice before resuspension in 500µL of cold PBS for analysis using flow cytometry (CytoFLEX 5, Beckman Coulter, Mississauga, ON, Canada) wherein mean fluorescence intensity of the gated cells (10,000

Cell line	Characteristic mutations	Culture media	Seeding density (cells/well)
OVCAR8	TP53[50], BRCA1 hypermethylation[51]	RPMI, 10% FBS, 100 units/mL penicillin and 100 µg/mL streptomycin	1000
HEYA8	PIK3CA, KRAS, BRAF[52]		1000
PEO1	TP53, BRCA2[32]		3000
PEO4	TP53[32]		3000

Table 3. Selected panel of human OC cell lines and their relevant mutations, culture conditions, and 96-well plate seeding densities used for in vitro combination cytotoxicity studies.

events) were collected and normalized to that of untreated cells (mean FITC treated divided by mean FITC untreated).

In vitro cellular uptake studies. Following analysis of FRα expression, the OVCAR8 and HEYA8 cell lines were selected as positive and negative controls, respectively. Liposomes passively loaded with the fluorescent probe calcein were prepared wherein HSPC, cholesterol, and DSPE-mPEG$_{2000}$ were mixed at a 55:40:4.75 molar ratio and dissolved in ethanol at 70 °C before direct hydration with 70 mM calcein buffer (70 mM calcein, 0.5 mM EDTA, 0.5 mM Tris in water, adjusted to pH 7.4 with 1 M NaOH). Calcein liposomes were then post-inserted with 0.25% molar of either folate-PEG$_{5k}$-DSPE or PEG$_{5k}$-DSPE as the folate receptor targeted and folate receptor untargeted formulations, respectively. Liposomes were purified by dialysis against HEPES buffered saline (HBS) for 24 hours until dialysis buffer showed no visually discernable trace of fluorescent colour. The OVCAR8 and HEYA8 cell lines were maintained in folate-free RPMI media, for a minimum of 5 passages to ensure they were folate starved prior to commencing uptake studies. Folate starved OVCAR8 and HEYA8 cell lines were plated onto 24-well plates at a seeding density of 1.24×10^5 cells per well and allowed to adhere prior to treatment with either folate conjugated or unconjugated liposomes at a lipid concentration of 100 μM phospholipid. Treated cells were then incubated at 37 °C for 1 h before triple wash with warm PBS. Washed cells were then scraped, collected, and analysed using flow cytometry as described above.

Formulation of unloaded liposomes. Unloaded liposomes were prepared using the following method. Briefly, HSPC, cholesterol, and PEG$_{2k}$-DSPE were mixed at a 55:40:4.75 molar ratio and dissolved in ethanol at 70 °C. TEA$_8$SOS buffer was prepared as described by Drummond et al. using ion exchange chromatography wherein the resultant free acid was titrated with neat triethylamine (TEA) to a pH of 5.7 prior to dilution to a final sulfate group concentration of 0.65 M[54]. TEA$_8$SOS buffer was then added to the dissolved lipids at 70 °C to achieve a final phospholipid concentration of 100 mM prior to being vortexed vigorously for two minutes to form multilamellar vesicles. The lipid mixture was then passed three times through double stacked, 0.2-micron pore size polycarbonate filters prior to extrusion through double stacked, 0.1-micron pore size polycarbonate filters (Whatman Inc., NJ, USA) 10 times using a 10 mL Lipex Extruder (Vancouver, BC, Canada) at 65 °C to make unilamellar liposomes. The resultant liposomes were then cooled on ice for 5 min before dialysis using a 50 kDa MWCO regenerated cellulose dialysis bag (Repligen, California, USA) overnight in pH 7.4 HBS at 4 °C.

Drug loading via active loading techniques. DOX and NIRB were dissolved in dimethyl sulfoxide (DMSO) and added to unloaded liposomes at a total concentration of 4% (v/v) DMSO and a 0.2 mol total drug:moles lipid (DL) ratio. Due to the limitations in allowable DMSO content, unloaded liposomes were diluted to an appropriate volume with HBS (pH 7.4) prior to addition of the drug solutions[55]. The resultant liposome and drug mixtures were then stirred at 65 °C for 1 hour before being cooled on ice for 5 min.

Post-insertion of folate targeting ligand. Addition of the folate targeting ligand was achieved using the post-insertion technique developed by Uster et al.[56]. In brief, folate-PEG$_{5k}$-DSPE was dissolved in HBS at 60 °C at a 5 mg/mL concentration. The folate-PEG$_{5k}$-DSPE solution was then added to the drug loaded liposomes such that the folate conjugated lipid accounted for 0.25% molar of the total lipid content. The liposomes were then stirred at 60 °C for 1 h. Resultant folate conjugated, drug loaded liposomes (NIRB-DOX-FA) were then purified by size exclusion chromatography (SEC) to remove free drug. Unconjugated control liposomes were post-inserted with PEG$_{5k}$-DSPE using the same technique as above. SEC columns were packed using Sepharose CL-4B purchased from GE Healthcare Bio-Sciences (Mississauga, ON, Canada). Purified liposomes were then either diluted or concentrated by tangential flow to relevant concentrations for use.

Analysis of NIRB and DOX. The concentrations of NIRB and DOX in samples were quantified using both HPLC–UV and MS analysis. Briefly, NIRB and DOX were extracted from liposome samples by tenfold dilution with methanol. The resultant samples were then centrifuged at 3000 RPM, 4 °C for 15 min in glass centrifuge tubes to separate extracted drug from lipid. The supernatant was then assayed directly for HPLC–UV or diluted accordingly for MS detection.

HPLC–UV analysis of samples was performed using an Agilent 1260 infinity series LC (Agilent Technologies, Santa Clara, CA, USA). Chromatographic separation was achieved using an Agilent Eclipse XDB-C18 column (4.6×150 mm, 5.0 μm) at 25 °C with a mobile phase composed of acetonitrile and methanol 50:50 (A) and 50 mM ammonium acetate, pH 4 (B). The initial mobile phase was 40% A with a flow rate of 1.0 mL/min, which was gradually increased to 55% A over 4 min. Following a 4-min equilibration, the composition was changed back to 40% A over a duration of 30 s. The mobile phase was then maintained for another 1.5 min until run completion. Detection of both drugs was achieved using an Agilent 1260 Infinity II Diode Array Detector with detection of NIRB and DOX at 310 nm and 480 nm wavelengths, respectively.

HPLC–MS analysis was performed using an Agilent 1260 infinity series LC equipped with an Agilent EC-C18 column (2.1×50 mm, 1.9 μM) heated to 40 °C. A gradient elution was applied using methanol (A) and water (B) both with 0.1% formic acid (v/v). The initial mobile phase was 75% A with a flow rate of 0.3 ml/min which was gradually decreased to 0% A over 4 min. This composition was maintained for another 6 min before it was rapidly changed back to 75% A where it was maintained for the remaining 3 min of the run.

Mass spectrometry detection of NIRB and DOX was achieved using a ThermoFisher Scientific TSQ Endura Triple Quadrupole Mass Spectrometer (Mississauga, ON, Canada). Analysis was performed on positive ion mode with optimal ion source settings as follows: spray voltage of 3500 V, sheath gas of 5 a.u., auxiliary gas of 2 a.u., and ion transfer tube temperature of 275 °C. Selected precursor ions for NIRB were m/z 321.2 → 180.0, 205.0,

207.0, 232.0, 304.083 while precursor ions for DOX were m/z 544.2 → 320.9, 345.9, 361.0, 378.9, 396.9. Collision energies ranged from 19.0 V to 42.0 V for NIRB and 11.2 V to 41.2 V for DOX.

The encapsulation efficiency of drug in liposomes was calculated using the following equation:

$$\%\ Encapsulation\ Efficiency = \frac{Drug\ Encapsulated\ (mg)}{Drug\ Added\ (mg)} \times 100\% \tag{5}$$

Lipid quantification. Quantification of HSPC and cholesterol was performed using an Agilent 1260 infinity series LC equipped with an Agilent evaporative light scattering detector (ELSD) operating at a 1.6 L/min gas flow with the evaporator and nebulizer heated to 80 °C and 50 °C, respectively. Lipids were extracted from liposome samples by direct dilution with methanol. Chromatographic separation of HSPC and cholesterol was achieved using an Eclipse XDB C18 column (150 × 4.6 mm, 5 µM) at 40 °C with mobile phase composed of methanol (A) and water (B) both with 0.1% trifluoroacetic acid (v/v). The initial mobile phase was 90% A with a flow rate of 1.0 mL/min, which was gradually increased to 100% A over 4 min. Following an 11-min equilibration, the composition was rapidly changed back to 90% A where it was maintained for the remaining 5 min of the run.

DL ratios were calculated using the following equation:

$$Moles\ Total\ Drug{:}\ Moles\ Lipid\ Ratio = \frac{Drug\ Encapsulated\ (moles)}{Phospholipid\ Content\ (moles)} \tag{6}$$

In vitro release of drugs. Evaluation of in vitro release of drugs from NIRB-DOX-FA was performed under sink conditions in 50 mg/mL of BSA(heat shock fraction, ≥ 98.0%, Sigma-Aldrich, Oakville, ON, Canada) in pH 7.4 HBS over five days at 37 °C. NIRB-DOX-FA liposomes were added to a BSA solution such that the final volume was 5 mL and the final concentration of NIRB and BSA were 1 mg/mL and 50 mg/mL, respectively. Samples of 100 µL were removed at pre-determined timepoints and purified by SEC to separate the liposomes from free drug. Sink conditions were maintained at all timepoints. NIRB and DOX were then extracted from BSA in the liposome fraction before analysis using HPLC–UV as described above.

Cryogenic transmission electron microscopy. Cryo-TEM imaging of NIRB-DOX-FA was performed at the University of Guelph Advanced Analytics Center. Liposome samples were diluted 50-fold with PBS and added to a Quantifoil Multi A holey carbon film (Quantifoil Micro Tools GmbH, Großlöbichau, Germany) deposited on a 300-mesh copper grid under humidity-controlled conditions at room temperature with excess sample removed prior to flash freezing with − 183 °C liquid ethane. Samples were then kept frozen by liquid nitrogen during the imaging process. Imaging was done using a FEI Tecnai G2 F20 microscope (FEI company, Hillsboro, OR, USA) equipped with a bottom mount Gatan 4 k CCD camera (Gatan Inc., Warrendale, PA, USA). Images were taken in bright field mode at a 200 kV acceleration voltage.

Gray intensity of the imaged space both inside and outside the liposomes was measured using ImageJ Version 1.8.0 (U. S. National Institutes of Health, Bethesda, U.S.A.) as mean gray area. Measurement of gray intensity was used to elucidate the physical state of the loaded drugs within the interior of the liposomes. The method used was adapted from the Cullis group[57]. Briefly, mean gray area expresses the gray intensity of all pixels in a selected area divided by the total number of pixels. Both internal and external areas of the imaged liposomes were sampled for mean gray area analysis. Internal mean gray values were then subtracted from external mean gray values to quantify the mean gray value difference across the bilayer. Approximately 50 liposomes were sampled from NIRB-DOX-FA images and compared to unloaded liposomes to elucidate the presence of concentrated NIRB-DOX deposits at the nanoparticle core.

Statistical analysis and relationship regressions. All statistical analyses were conducted using GraphPad Prism version 9.0. Mean gray value differences between loaded and unloaded liposomes were compared using unpaired t-tests. In addition, differences in FRα expression in the panel of OC cell lines were compared using one-way ANOVA and Tukey's multiple comparisons test while differences in cellular uptake between folate conjugated and unconjugated liposomes in the same cell line were analyzed using paired t-tests.

All linear and non-linear regressions were produced using GraphPad Prism version 9.0. Non-linear regression curve fitting equations selected for relationship modeling include Prism version 9.0's built-in "exponential growth equation", "third order polynomial (cubic)", and "second order polynomial (quadratic)" parameters. Informed selection of constrained versus unconstrained regressions was made using GraphPad Prism's "Comparison of Fits" analysis.

Data availability

Data generated and analysed throughout the duration of this study are available upon request from the corresponding author.

Received: 30 August 2022; Accepted: 18 January 2023
Published online: 24 February 2023

References

1. Canadian Cancer Statistics Advisory Committee. *Canadian Cancer Statistics 2021*, Can. Cancer Soc. Stat. Canada Public Heal. Agency Canada (2021) 1–95.
2. The American Cancer Society. *Key Statistics for Ovarian Cancer*. Am. Cancer Soc. (2022) 1. https://www.cancer.org/cancer/ovarian-cancer/about/key-statistics.html.
3. NIH National Cancer Institute. *Cancer Stat Facts: Ovarian Cancer* (2022). https://seer.cancer.gov/statfacts/html/ovary.html.
4. Kim, G. *et al.* FDA approval summary: Olaparib monotherapy in patients with deleterious germline BRCA-mutated advanced ovarian cancer treated with three or more lines of chemotherapy. *Clin. Cancer Res.* **21**, 4257–4261. https://doi.org/10.1158/1078-0432.CCR-15-0887 (2015).
5. AstraZenica, Lynparza Monograph, 2022.
6. Muggia, F., Safra, T. & Aviv, T. BRCAness and its implications for platinum action in gynecologic cancer. *Anticancer Res.* **34**, 551–556 (2014).
7. Helleday, T. The underlying mechanism for the PARP and BRCA synthetic lethality: Clearing up the misunderstandings. *Mol. Oncol.* **5**, 387–393. https://doi.org/10.1016/j.molonc.2011.07.001 (2011).
8. Murai, J. *et al.* Differential trapping of PARP1 and PARP2 by clinical PARP inhibitors. *Cancer Res.* **72**, 5588–5599. https://doi.org/10.1158/0008-5472.CAN-12-2753.Differential (2013).
9. Murthy, P. & Muggia, F. PARP inhibitors: Clinical development, emerging differences, and the current therapeutic issues. *Cancer Drug Resist.* https://doi.org/10.20517/cdr.2019.002 (2019).
10. Dent, R. A. *et al.* Phase I trial of the oral PARP inhibitor olaparib in combination with paclitaxel for first- or second-line treatment of patients with metastatic triple-negative breast cancer. *Breast Cancer Res.* https://doi.org/10.1186/bcr3484 (2013).
11. Balmaña, J. *et al.* Phase I trial of olaparib in combination with cisplatin for the treatment of patients with advanced breast, ovarian and other solid tumors. *Ann. Oncol.* **25**, 1656–1663. https://doi.org/10.1093/annonc/mdu187 (2014).
12. Rajan, A. *et al.* A phase I combination study of olaparib with cisplatin and gemcitabine in adults with solid tumors. *Clin. Cancer Res.* **18**, 2344–2351. https://doi.org/10.1158/1078-0432.CCR-11-2425 (2012).
13. Kunos, C. *et al.* A phase I-II evaluation of veliparib (NSC #737664), topotecan, and filgrastim or pegfilgrastim in the treatment of persistent or recurrent carcinoma of the uterine cervix: An NRG oncology/gynecologic oncology group study. *Int. J. Gynecol. Cancer.* **25**, 484–492. https://doi.org/10.1097/IGC.0000000000000380 (2015).
14. Lee, J. M. *et al.* Sequence-specific pharmacokinetic and pharmacodynamic phase I/Ib study of olaparib tablets and carboplatin in women's cancer. *Clin. Cancer Res.* **23**, 1397–1406. https://doi.org/10.1158/1078-0432.CCR-16-1546 (2017).
15. Lampert, E. J. *et al.* Phase I/Ib study of olaparib and carboplatin in heavily pretreated recurrent high-grade serous ovarian cancer at low genetic risk. *Oncotarget* **10**, 2855–2868. https://doi.org/10.18632/oncotarget.26869 (2019).
16. Xu, J. *et al.* Phase II trial of veliparib and temozolomide in metastatic breast cancer patients with and without BRCA1/2 mutations. *Breast Cancer Res. Treat.* **189**, 641–651. https://doi.org/10.1007/s10549-021-06292-7 (2021).
17. Matulonis, U. A. & Monk, B. J. PARP inhibitor and chemotherapy combination trials for the treatment of advanced malignancies: Does a development pathway forward exist?. *Ann. Oncol.* **28**, 443–447. https://doi.org/10.1093/annonc/mdw697 (2017).
18. Oza, A. M. *et al.* Olaparib combined with chemotherapy for recurrent platinum-sensitive ovarian cancer: A randomised phase 2 trial. *Lancet Oncol.* **16**, 87–97. https://doi.org/10.1016/S1470-2045(14)71135-0 (2015).
19. Roulston, A. *et al.* RP-3500: A novel, potent, and selective ATR inhibitor that is effective in preclinical models as a monotherapy and in combination with PARP inhibitors. *Mol. Cancer Ther.* **21**, 245–256. https://doi.org/10.1158/1535-7163.MCT-21-0615 (2022).
20. Fang, Y. *et al.* Sequential therapy with PARP and WEE1 inhibitors minimizes toxicity while maintaining efficacy. *Cancer Cell.* **35**, 851-867.e7. https://doi.org/10.1016/j.ccell.2019.05.001 (2019).
21. Meng, H. *et al.* Use of a lipid-coated mesoporous silica nanoparticle platform for synergistic gemcitabine and paclitaxel delivery to human pancreatic cancer in mice. *ACS Nano* **9**, 3540–3557. https://doi.org/10.1021/acsnano.5b00510 (2015).
22. Zhang, J. *et al.* Synergistic anti-tumor effects of combined gemcitabine and cisplatin nanoparticles in a stroma-rich bladder carcinoma model. *J. Control. Release* **182**, 90–96. https://doi.org/10.1016/j.jconrel.2014.03.016 (2014).
23. Liu, H. *et al.* Arsenite-loaded nanoparticles inhibit PARP-1 to overcome multidrug resistance in hepatocellular carcinoma cells. *Sci. Rep.* **6**, 1–13. https://doi.org/10.1038/srep31009 (2016).
24. Tardi, P. *et al.* In vivo maintenance of synergistic cytarabine: Daunorubicin ratios greatly enhances therapeutic efficacy. *Leuk. Res.* **33**, 129–139. https://doi.org/10.1016/j.leukres.2008.06.028 (2009).
25. Krauss, A. C. *et al.* FDA approval summary: (Daunorubicin and cytarabine) liposome for injection for the treatment of adults with high-risk acute myeloid leukemia. *Clin. Cancer Res.* **25**, 2685–2690. https://doi.org/10.1158/1078-0432.CCR-18-2990 (2019).
26. Petersen, G. H., Alzghari, S. K., Chee, W., Sankari, S. S. & La-Beck, N. M. Meta-analysis of clinical and preclinical studies comparing the anticancer efficacy of liposomal versus conventional non-liposomal doxorubicin. *J. Control. Release* **232**, 255–264. https://doi.org/10.1016/j.jconrel.2016.04.028 (2016).
27. Kolitz, J. E. *et al.* Consolidation outcomes in CPX-351 versus cytarabine/daunorubicin-treated older patients with high-risk/secondary acute myeloid leukemia. *Leuk. Lymphoma* **61**, 631–640. https://doi.org/10.1080/10428194.2019.1688320 (2020).
28. Kalli, K. R. *et al.* Folate receptor alpha as a tumor target in epithelial ovarian cancer. *Gynecol. Oncol.* **108**, 619–626. https://doi.org/10.1038/jid.2014.371 (2008).
29. W.S. Rasband, U.S. National Institutes of Health. *ImageJ* (2018). https://imagej.nih.gov/ij/.
30. Eetezadi, S. *et al.* Ratio-dependent synergism of a doxorubicin and olaparib combination in 2D and spheroid models of ovarian cancer. *Mol. Pharm.* **15**, 472–485. https://doi.org/10.1021/acs.molpharmaceut.7b00843 (2018).
31. Sun, K. *et al.* A comparative pharmacokinetic study of PARP inhibitors demonstrates favorable properties for niraparib efficacy in preclinical tumor models. *Oncotarget* **9**, 37080–37096. https://doi.org/10.18632/oncotarget.26354 (2018).
32. Langdon, S. P. *et al.* Characterization and properties of nine human ovarian adenocarcinoma cell lines. *Cancer Res.* **48**, 6166–6172 (1988).
33. Sakai, W. *et al.* Functional restoration of BRCA2 protein by secondary BRCA2 mutations in BRCA2-mutated ovarian carcinoma. *Cancer Res.* **69**, 6381–6386. https://doi.org/10.1158/0008-5472.CAN-09-1178 (2009).
34. Roy, R., Chun, J. & Powell, S. N. BRCA1 and BRCA2: Different roles in a common pathway of genome protection. *Nat. Rev. Cancer* **12**, 68–78. https://doi.org/10.1038/nrc3181 (2012).
35. Del Conte, G. *et al.* Phase I study of olaparib in combination with liposomal doxorubicin in patients with advanced solid tumours. *Br. J. Cancer* **111**, 651–659. https://doi.org/10.1038/bjc.2014.345 (2014).
36. Lheureux, S. *et al.* Somatic BRCA1/2 recovery as a resistance mechanism after exceptional response to poly (ADP-ribose) polymerase inhibition. *J. Clin. Oncol.* **35**, 1240–1249. https://doi.org/10.1200/JCO.2016.71.3677 (2017).
37. Wang, L., Li, M. & Zhang, N. Folate-targeted docetaxel-lipid-based-nanosuspensions for active-targeted cancer therapy. *Int. J. Nanomed.* **7**, 3281–3294. https://doi.org/10.2147/IJN.S32520 (2012).
38. Chaudhury, A., Das, S., Bunte, R. M. & Chiu, G. N. C. Potent therapeutic activity of folate receptor-targeted liposomal carboplatin in the localized treatment of intraperitoneally grown human ovarian tumor xenograft. *Int. J. Nanomed.* **7**, 739–751. https://doi.org/10.2147/IJN.S26172 (2012).
39. Tong, L., Chen, W., Wu, J. & Li, H. Folic acid-coupled nano-paclitaxel liposome reverses drug resistance in SKOV3/TAX ovarian cancer cells. *Anticancer Drugs* **25**, 244–254. https://doi.org/10.1097/CAD.0000000000000047 (2014).

40. Moore, K. N. *et al.* Phase III, randomized trial of mirvetuximab soravtansine versus chemotherapy in patients with platinum-resistant ovarian cancer: Primary analysis of FORWARD I. *Ann. Oncol.* **32**, 757–765. https://doi.org/10.1016/j.annonc.2021.02.017 (2021).
41. Li, T., Cipolla, D., Rades, T. & Boyd, B. J. Drug nanocrystallisation within liposomes. *J. Control. Release* **288**, 96–110. https://doi.org/10.1016/j.jconrel.2018.09.001 (2018).
42. Abraham, S. A. *et al.* Formation of transition metal-doxorubicin complexes inside liposomes. *Biochim. Biophys. Acta Biomembr.* **1565**, 41–54. https://doi.org/10.1016/S0005-2736(02)00507-2 (2002).
43. Drummond, D. C., Kirpotin, D. B., Hayes, M. E., Noble, C., Kesper, K., Awad, A. M., Moore, D. J., & O'Brien, A. J. *Liposomal Irinotecan Preparations*. US Patent 2018/0110771 A1 (2018).
44. Yang, W. *et al.* The influence of trapping agents on the antitumor efficacy of irinotecan liposomes: Head-to-head comparison of ammonium sulfate, sulfobutylether-β-cyclodextrin and sucrose octasulfate. *Biomater. Sci.* **7**, 419–428. https://doi.org/10.1039/c8bm01175c (2019).
45. Swenson, C. E., Perkins, W. R., Roberts, P. & Janoff, A. S. Liposome technology and the development of Myocet™ (liposomal doxorubicin citrate). *Breast* **10**, 1–7. https://doi.org/10.1054/brst.2000.0201 (2001).
46. Johnston, M. J. W., Edwards, K., Karlsson, G. & Cullis, P. R. Influence of drug-to-lipid ratio on drug release properties and liposome integrity in liposomal doxorubicin formulations. *J. Liposome Res.* **18**, 145–157. https://doi.org/10.1080/08982100802129372 (2008).
47. Hendriks, B. S. *et al.* Impact of tumor HER2/ERBB2 expression level on HER2-targeted liposomal doxorubicin-mediated drug delivery: Multiple low-affinity interactions lead to a threshold effect. *Mol. Cancer Ther.* **12**, 1816–1828. https://doi.org/10.1158/1535-7163.MCT-13-0180 (2013).
48. Reynolds, J. G. *et al.* HER2-targeted liposomal doxorubicin displays enhanced anti-tumorigenic effects without associated cardiotoxicity. *Toxicol. Appl. Pharmacol.* **262**, 1–10. https://doi.org/10.1016/j.taap.2012.04.008 (2012).
49. Chou, T. & Talalay, P. Quantitative analysis of dose-effect relationships: The combined effects of multiple drugs or enzyme inhibitors. *Adv. Enzyme Regul.* **66**, 27–55. https://doi.org/10.1016/0065-2571(84)90007-4 (1984).
50. Schilder, R. J. *et al.* Metallothionein gene expression and resistance to cisplatin in human ovarian cancer. *Int. J. Cancer* **45**, 66 (1990).
51. Shen, Y. T., Wang, L., Evans, J. C., Allen, C. & Piquette-Miller, M. Development of a bioluminescent BRCA1-deficient xenograft model of disseminated, high-grade serous ovarian cancer. *Int. J. Mol. Sci.* **20**, 1–13. https://doi.org/10.3390/ijms20102498 (2019).
52. Domcke, S. *et al.* Evaluating cell lines as tumour models by comparison of genomic profiles. *Nat. Commun.* **4**, 66. https://doi.org/10.1038/ncomms3126 (2013).
53. Sonvico, F. *et al.* Establishment of an in vitro model expressing the folate receptor for the investigation of targeted delivery systems. *J. Drug Deliv. Sci. Technol.* **15**, 407–410. https://doi.org/10.1016/s1773-2247(05)50080-7 (2005).
54. Drummond, D. C. *et al.* Development of a highly active nanoliposomal irinotecan using a novel intraliposomal stabilization strategy. *Cancer Res.* **66**, 3271–3277. https://doi.org/10.1158/0008-5472.CAN-05-4007 (2006).
55. Hayes, I. M. E., Francisco, S., Us, C. A., Szoka, F. C. United States Patent No. US 9,737,485 B2 (2017).
56. Uster, P. S. *et al.* Insertion of poly(ethylene glycol) derivatized phospholipid into pre-formed liposomes results in prolonged in vivo circulation time. *FEBS Lett.* **386**, 243–246. https://doi.org/10.1016/0014-5793(96)00452-8 (1996).
57. Semple, S. C. *et al.* Optimization and characterization of a sphingomyelin/cholesterol liposome formulation of vinorelbine with promising antitumor activity. *J. Pharm. Sci.* **94**, 1024–1038. https://doi.org/10.1002/jps.20332 (2005).

Acknowledgements

These studies were funded by the Department of Defense (Award number W81XWH-16-1-0388) and the Nanomedicines Innovation Network (NMIN). L.W. and L.A. acknowledge support from NSERC CREATE. L.W acknowledges scholarships from the Centre for Pharmaceutical Oncology (CPO). The authors acknowledge use of equipment in the CPO in the Leslie Dan Faculty of Pharmacy at the University of Toronto. The authors also acknowledge the valued contributions of Maximillian Regenold and Linyu Fan.

Author contributions

L.W.: Conceptualization, Methodology, Validation, Formal Analysis, Investigation, Writing—Original Draft, Visualization; J.E.: Writing—Review and Editing, Project Administration; L.A.: Investigation, Writing—Review and Editing; C.A.: Conceptualization, Writing—Review and Editing, Funding Acquisition, Supervision.

Competing interests

The authors declare no competing interests.

Additional information

Supplementary Information The online version contains supplementary material available at https://doi.org/10.1038/s41598-023-28424-3.

Correspondence and requests for materials should be addressed to C.A.

Reprints and permissions information is available at www.nature.com/reprints.

Publisher's note Springer Nature remains neutral with regard to jurisdictional claims in published maps and institutional affiliations.

Open Access This article is licensed under a Creative Commons Attribution 4.0 International License, which permits use, sharing, adaptation, distribution and reproduction in any medium or format, as long as you give appropriate credit to the original author(s) and the source, provide a link to the Creative Commons licence, and indicate if changes were made. The images or other third party material in this article are included in the article's Creative Commons licence, unless indicated otherwise in a credit line to the material. If material is not included in the article's Creative Commons licence and your intended use is not permitted by statutory regulation or exceeds the permitted use, you will need to obtain permission directly from the copyright holder. To view a copy of this licence, visit http://creativecommons.org/licenses/by/4.0/.

© The Author(s) 2023